

# COMPARATIVE STUDY OF NUMERICAL SCHEMES EMPLOYING THE SEMI-STAGGERED MESH FOR THE BACKWARD FACING STEP TEST PROBLEM

Kéteri Poliane Moraes de Oliveira, [keteri19@yahoo.com.br](mailto:keteri19@yahoo.com.br)

José Ricardo Figueiredo, [jrfigue@fem.unicamp.br](mailto:jrfigue@fem.unicamp.br)

University State of Campinas - UNICAMP

Mechanical Engineering Faculty – Energy Department

PO Box: 6122 – Zip Code: 13083-970 – Campinas – SP – Brazil

**Abstract.** *This work presents a comparison of the accuracy of the numerical schemes central differencing and UNIFAES (Unified Finite Approaches Exponential-type Scheme) for the discretization of the advective and viscous terms of the incompressible Navier-Stokes equations in primitive variables, employing the semi-staggered mesh. The backward facing step test problems are used. Several mesh refinements and Reynolds numbers are tested. Richardson extrapolation is employed to estimate the correct solution in cases which have no precise reference solution. For the backward facing step problem, it was possible to solve the non diagonally dominant pressure equation of the semi-staggered mesh by iterative method employing an appropriate under-relaxation factor. For Reynolds numbers above 600, the numerical results with both UNIFAES and central differencing schemes became crescently distinct of the experimental results found in the literature, which can be attributed to three-dimensional effects of the experiments. UNIFAES proved to be stable even at higher values of the Reynolds number, and more accurate than the central differencing.*

**Keywords:** *Discretization schemes, UNIFAES, Incompressible fluid, semi- staggered mesh, backward facing step.*

## 1. INTRODUCTION

The present paper deals with the two-dimensional modeling of the backward facing step flow, employing the semi-staggered mesh, originally presented by Kuznetsov (1968), but which remains rarely used in the Finite Volume literature in comparison with the staggered and the cell-center collocated meshes. The time-wise integration of the incompressible Navier-Stokes is explicit. Three different discretization schemes are used for discretizing the advective and viscous transport terms: central differencing and UNIFAES. These schemes were extensively compared in the moving lid cavity flow, Figueiredo e Oliveira (2009a, b), where UNIFAES was shown to combine accuracy superior to the other schemes.

In the cited references, using square meshes, the accuracy of the semi-staggered mesh is comparable to that of the staggered and the collocated meshes. For the reasons explained below, the semi-staggered mesh is much more affected than the others by non square meshes. Therefore, the backward facing-step flow, which is a well known test problem with the characteristic feature of demanding cells with very high aspect ratios, i.e,  $\Delta x$  much greater than  $\Delta y$ , was chosen to investigate this seldom used mesh.

More information can be viewed on the doctoral thesis of Oliveira, K. P. M. (2009).

## 2. METHODOLOGY

### 2.1. Mathematical equations

The governing equations for incompressible flows in 2D Cartesian geometries are presented below. The continuity equation is reduced to null dilation, i.e., null divergent of the velocity field:

$$\frac{\partial u}{\partial x} + \frac{\partial v}{\partial y} = 0 \quad (1)$$

The Navier-Stokes equations are expressed for simplicity as:

$$\frac{\partial u}{\partial t} = A_u - \frac{\partial P}{\partial x} \quad \text{e} \quad \frac{\partial v}{\partial t} = A_v - \frac{\partial P}{\partial y} \quad (2)$$

where  $A_u$  e  $A_v$  represent the combined advective and viscous net flux of the  $x$  and  $y$  momentum components, given in conservative form, given below in terms of a dummy variable  $\phi$ :

$$A_\varphi = \text{Re} \frac{\partial (u\varphi)}{\partial x} + \text{Re} \frac{\partial (v\varphi)}{\partial y} - \frac{\partial^2 \varphi}{\partial x^2} - \frac{\partial^2 \varphi}{\partial y^2} \quad (3)$$

In the equations above, the spatial coordinates  $x$  and  $y$  were made non-dimensional by means of a characteristic length  $L_c$ , the velocity components  $u$  and  $v$  by a characteristic velocity  $V_c$ , and time  $t$  by  $\text{Re} L_c / V_c$ , where the Reynolds number is defined as  $\text{Re} = \rho V_c L_c / \mu$ . The pressure-like term  $P$  is the sum of the physical pressure  $P_{ph}$  and the hydrostatic head  $\rho g z$ , made non-dimensional by the factor  $\mu V_{ch} / L_{ch}$ .

Figure 1 sketches the semi-staggered mesh structure employed herein. Two mass control volumes are illustrated. The solid line represents the locations associated to integer value in the notation below.

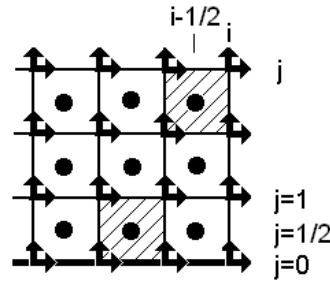


Figure 1 – Semi-staggered mesh.

In the semi-staggered structure, Fig. 1, the pressure is located at the center of the continuity control-volume and both velocity components are collocated at its vertices. Filling entirely a rectangular domain with regular continuity control volumes automatically guarantees regularly spaced grids for both momentum components. The divergent of the velocity is:

$$D_{i-1/2, j-1/2}^n = \frac{u_{i,j}^n + u_{i,j-1}^n - u_{i-1,j}^n - u_{i-1,j-1}^n}{2 \Delta x} + \frac{v_{i,j}^n + v_{i-1,j}^n - v_{i,j-1}^n - v_{i-1,j-1}^n}{2 \Delta y} = 0 \quad (4)$$

The momentum conservation equations are discretized explicitly in time in the form:

$$\frac{u_{i,j}^{n+1} - u_{i,j}^n}{\Delta t} = A_{u,i,j}^n - \frac{P_{i+1/2, j-1/2}^n + P_{i+1/2, j+1/2}^n - P_{i-1/2, j-1/2}^n - P_{i-1/2, j+1/2}^n}{2 \Delta x} \quad (5)$$

$$\frac{v_{i,j}^{n+1} - v_{i,j}^n}{\Delta t} = A_{v,i,j}^n - \frac{P_{i+1/2, j+1/2}^n + P_{i-1/2, j+1/2}^n - P_{i+1/2, j-1/2}^n - P_{i-1/2, j-1/2}^n}{2 \Delta y} \quad (6)$$

Taking the numerical divergent of the vector equation (5)-(6) by analogy with the divergent of the velocity in Eq. (4), the resulting Poisson equation for the pressure is:

$$\begin{aligned} & - \left( \frac{1}{(\Delta x)^2} + \frac{1}{(\Delta y)^2} \right) P_{i-1/2, j-1/2}^n + \left( \frac{0.25}{(\Delta x)^2} + \frac{0.25}{(\Delta y)^2} \right) \left( P_{i-3/2, j+1/2}^n + P_{i+1/2, j-3/2}^n + P_{i+1/2, j+1/2}^n + P_{i-3/2, j-3/2}^n \right) + \\ & + \left( \frac{0.5}{(\Delta x)^2} - \frac{0.5}{(\Delta y)^2} \right) \left( P_{i+1/2, j-1/2}^n + P_{i-3/2, j-1/2}^n - P_{i-1/2, j+1/2}^n - P_{i-1/2, j-3/2}^n \right) = \\ & = \frac{A_{u,i,j}^n + A_{u,i,j-1}^n - A_{u,i-1,j}^n - A_{u,i-1,j-1}^n}{2 \Delta x} + \frac{A_{v,i,j}^n + A_{v,i-1,j}^n - A_{v,i,j-1}^n - A_{v,i-1,j-1}^n}{2 \Delta y} - \frac{D_{i-1/2, j-1/2}^{n+1} - D_{i-1/2, j-1/2}^n}{\Delta t} \end{aligned} \quad (7)$$

As usual,  $D_{i-1/2, j-1/2}^{n+1}$  is put zero and  $D_{i-1/2, j-1/2}^n$  is computed as (4).

The pressure equation (7) is generally not diagonally dominant, except in the case  $\Delta x = \Delta y$ , in which the influence coefficients of the nodes  $(i-1/2 \pm 1, j-1/2)$  and  $(i-1/2, j-1/2 \pm 1)$  vanish so that the central node  $(i-1/2, j-1/2)$  becomes dependent on the nodes  $(i-1/2 \pm 1, j-1/2 \pm 1)$  only.

The system of pressure equations is closed by using the velocities imposed at the boundaries in the neighboring continuity control volumes. Therefore, all pressure nodes are internal to the domain and no explicit pressure boundary condition is required.

### 2.3. Figures and tables

The choice of domain was based on the work of Armaly *et al.* (1983), which is often cited in literature as a reference work. The experimental set had, the dimensions  $h = 5,2$  mm e  $S = 4,9$  mm:

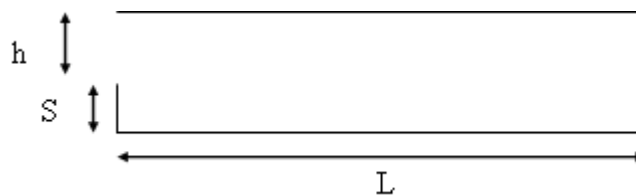


Figure 2 – Sketch of backward facing step with the dimensions of the Armaly *et al.* (1983)’s work.

To maintain the same proportions of this work, we chose the height of the step so that they could divide whole into parts of equal length and with roughly the same rate of expansion, ie,  $5.2/10.1 \cong 17/33$ . This is explained as follows. The difference between 5.2 and 4.9, ie 0.3, was taken as the highest possible cell size. If we divide the domain high for this value there will be approximately 33 units. From this account, we have chosen the mesh refinement in the vertical direction as 33 pitches and its multiples 66, 99, etc.

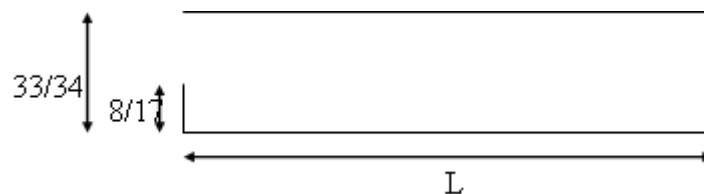


Figure 3 – Sketch of flow backward facing step with the dimensions.

The geometry has  $[0, L] \times [0, 33/34]$  as dimension. Two different values were chosen for the length  $L$ :  $L = 10$ : for Reynolds numbers between 100 and 700 and  $L = 15$  for Reynolds numbers between 800 and 1200. The criterion for defining the length of the channel was based on comparing the effect of different lengths on the size of the bubbles, as shown in Table 1.

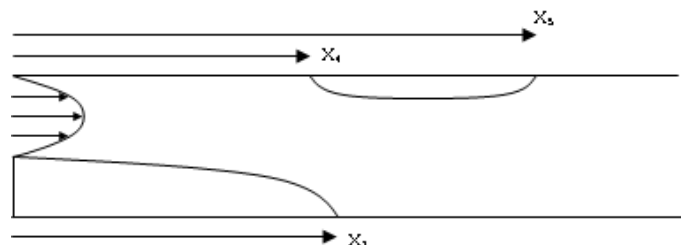


Figure 4 – Sketch of  $X_1$ ,  $X_4$  e  $X_5$  lengths.

Tests were performed with various meshes while keeping the cell size and increasing the domain. Through these tests, we could see that for the first bubble a change in channel length from 10 to 20 did not interfere with the lengths  $X_1$ ,  $X_4$  e  $X_5$  until Reynolds 800, i.e., the profile had shown to be developed. Because of the second bubble it

was necessary to increase the channel length for Reynolds equal and above 800 to about 15. These results are shown in the table 1:

Table 1 – bubble lengths results.

semi-staggered mesh				
Reynolds	channel lengths	bubble lengths		
		$X_1 / S$	$X_4 / S$	$X_5 / S$
100	10,0(33x33)	3,23878	-----	-----
	20,0(66x33)	3,23878	-----	-----
500	10,0 (66x66)	9,53269	8,38653	13,02188
	20,0 (132x66)	9,53272	8,38654	13,02188
800	15,15 (50x33)	12,07873	10,19506	19,80813
	20,0(67x33)	12,07872	10,19506	19,80813
1200	15,15 (150x99)	13,83799	11,00957	28,52413
	20,0(198x99)	13,83799	11,00957	28,45258

Because of the lack of diagonal dominance of the pressure equation of semi-staggered mesh in non square grids, the following sub-relaxation factor was used for the pressure equation:

$$w = \frac{\left| \frac{1}{\Delta x^2} + \frac{1}{\Delta y^2} \right|}{\left| \frac{1}{\Delta x^2} + \frac{1}{\Delta y^2} \right| + \left| \frac{2}{\Delta x^2} - \frac{2}{\Delta y^2} \right|} \quad (8)$$

which approaches 1/3 when  $\Delta x \gg \Delta y$ .

The definition of Reynolds number, following Armaly *et al.* (1983) and many others, is:

$$Re = \frac{VD}{\nu} \quad (9)$$

where V is two-thirds of the velocity maximum input, which corresponds in the laminar case to the average velocity of input, D is the hydraulic diameter of the entrance (small) and corresponds to twice their high,  $D = 2h$ , and  $\nu$  is the kinematic viscosity.

All wall boundaries are impermeable and adherent. For the velocity, in the walls and in the channel entrance Dirichlet boundary conditions were used, while in the outlet homogeneous Newman condition is assumed,  $x = L$  and  $0 \leq y \leq 33/34$ .

At the entrance, a fully developed laminar profile was assumed leading to the velocity shown in Eq. (10)

In  $x = 0$  and  $8/17 \leq y \leq 33/34$

$$u = -6 \left( 4y^2 - \frac{98}{17}y + \frac{528}{289} \right) \quad \text{and} \quad v = 0 \quad (10)$$

The system of pressure equations was closed using the values of the velocity of the border, even in the outlet, where the velocity vary throughout the iterative process. The pressure Poisson equation is solved iteratively with 200 Gauss-Siedel sweeps for each time-wise iteration. The Rhie and Chow (1983) momentum interpolation was used as post processing to eliminate the oscillations of the pressure field.

Figure (5) to (14) show the streamlines and pressure graphics for various Reynolds numbers. Figures show that consistent with the literature.

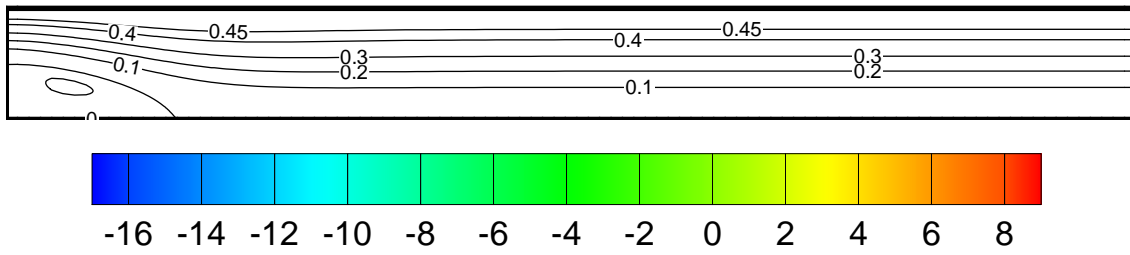


Figure 5 – Streamlines (above) and pressure (below) for  $Re = 100$  with central scheme

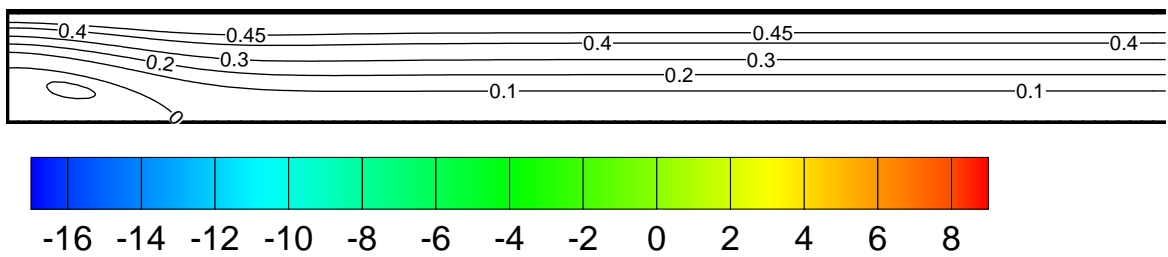


Figure 6 – Streamlines (above) and pressure (below) for  $Re = 100$  with UNIFAES.

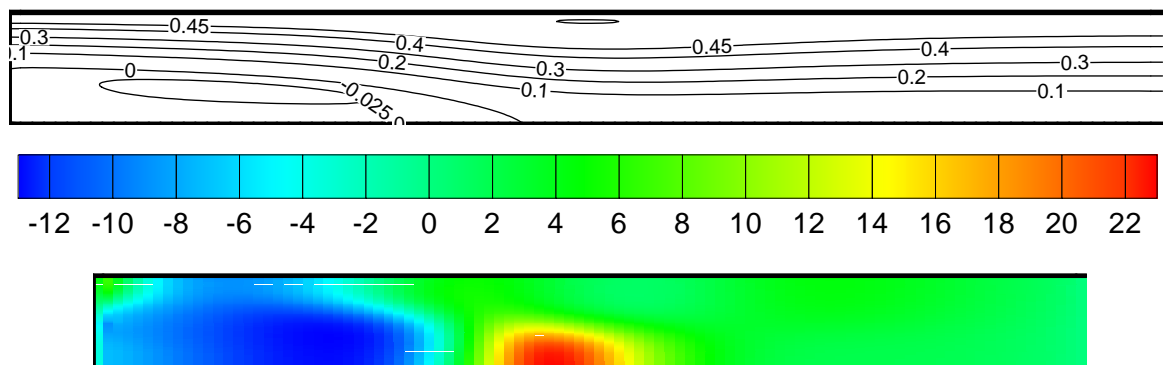


Figure 7 - Streamlines (above) and pressure (below) for  $Re = 500$  with central scheme

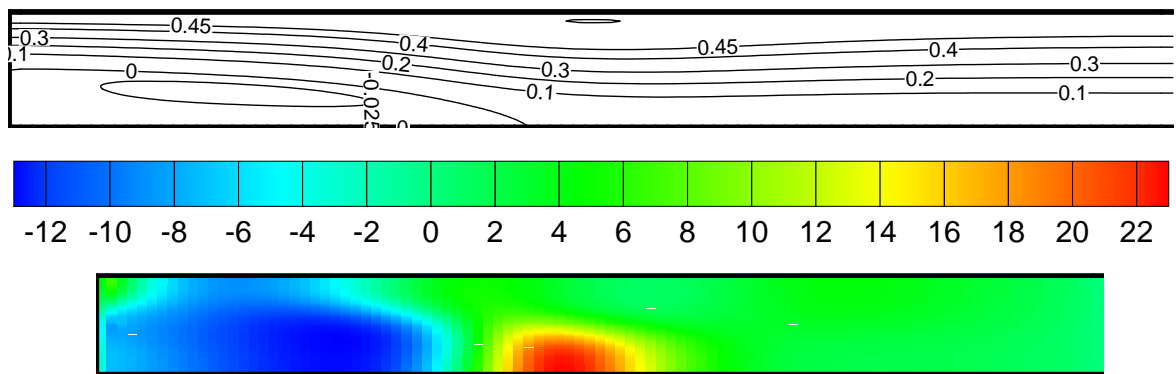


Figure 8 – Streamlines (above) and pressure (below) for  $Re = 500$  with UNIFAES.

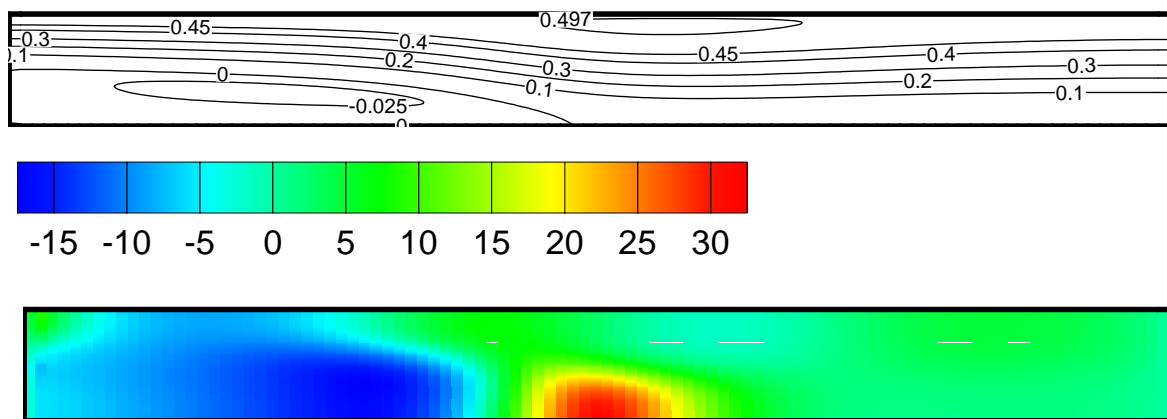


Figure 9 - Streamlines (above) and pressure (below) for  $Re = 600$  with central scheme.

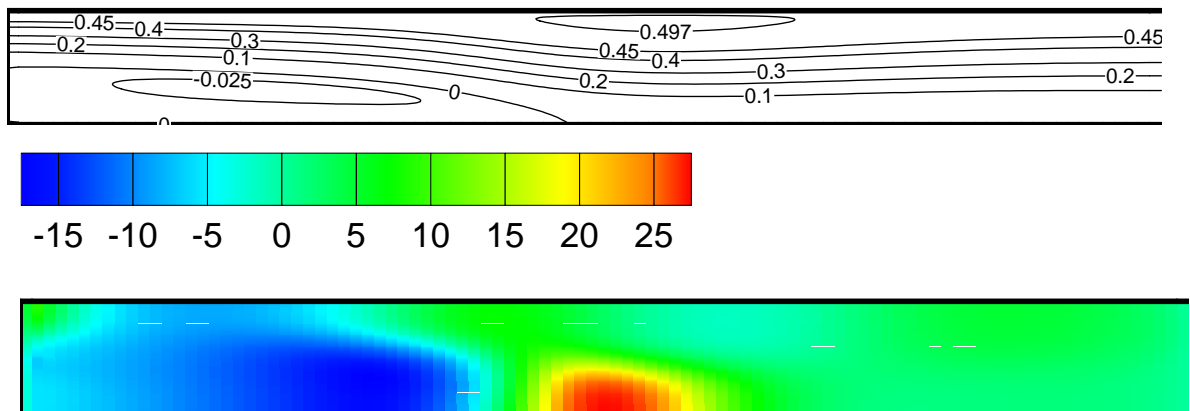


Figure 10 – Streamlines (above) and pressure (below) for  $Re = 600$  with UNIFAES.

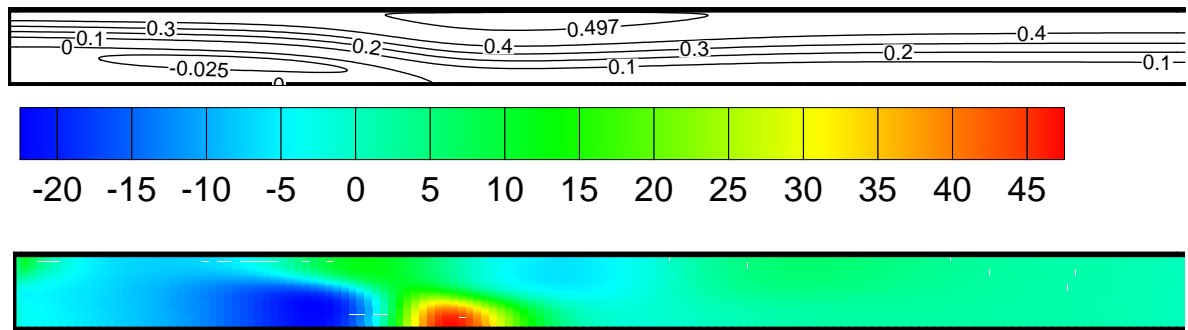


Figure 11 - Streamlines (above) and pressure (below) for  $Re = 800$  with central scheme.

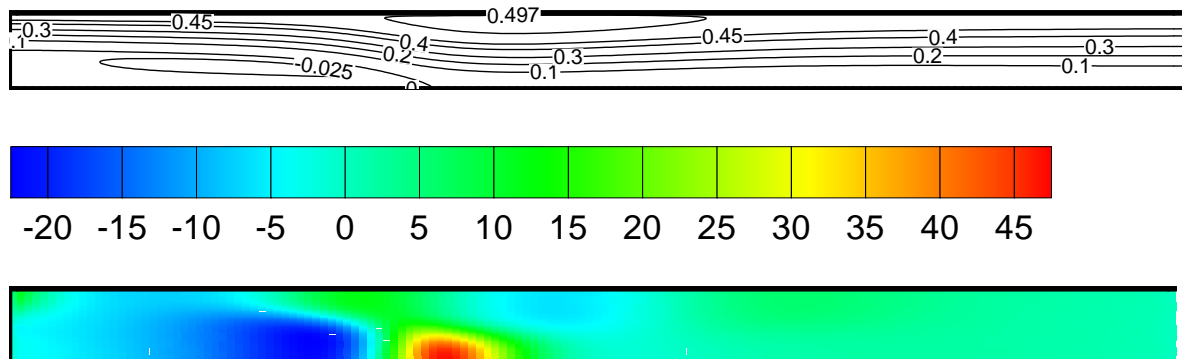


Figure 2 - Streamlines (above) and pressure (below) for  $Re = 800$  with UNIFAES.

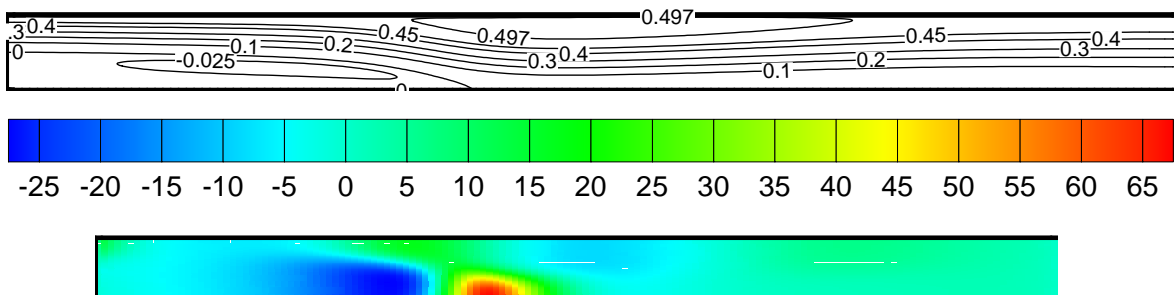


Figure 13 - Streamlines (above) and pressure (below) for  $Re = 1000$  with UNIFAES.

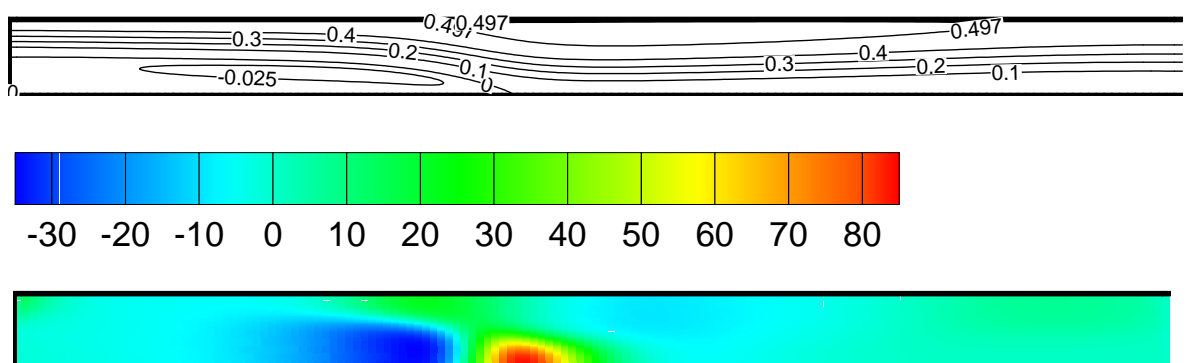


Figure 14 - Streamlines (above) and pressure (below) for  $Re = 1200$  with UNIFAES.

Figure (15) shows the experimental results of Armaly *et al.* (1983) and the present numerical results for the  $X_1$ ,  $X_4$  e  $X_5$  lengths.

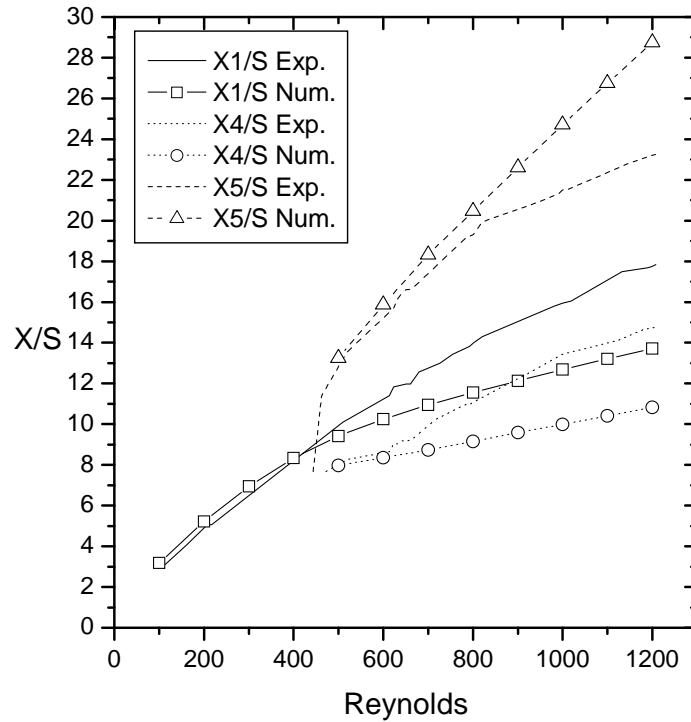


Figure 15 - Evolution of bubble length with Reynolds number. Experimental results of Armaly *et al.* (1983) and present numerical results.

Table 2 shows the extrapolated results of the computations with the schemes central differencing and UNIFAES for lengths data  $X_1$ ,  $X_4$  e  $X_5$ , following the notation used by Armaly *et al.* (1983). Mesh refinements 66x66 and 99x99 were employed up to  $Re = 700$  and 99x66 and 150x99 from  $Re = 800$  on. For the first bubble, there is excellent agreement between both extrapolations for low Reynolds numbers, with differences below 0,1%; the distinction between them increasing up to almost 1% for Reynolds number 800. The reattachment point of the second bubble also presents differences of less than 1%, but the beginning of this bubble is much more uncertain, with differences up to 3%.

As shown in these figures and in the table, for Reynolds number 600 and higher, an increasing difference can be seen between the experimental results of Armaly *et al.* (1983) and both present numerical results. That difference is attributed to the fact that the flow becomes three dimensional.

Table 2 – Extrapolated results to the values  $X_1$ ,  $X_4$  e  $X_5$  using semi-staggered mesh with central, exponential and UNIFAES schemes.

Scheme Bubble length	Reynolds	Extrapolations		
		Central	Unifaes	Armaly
Length of $X_1 / S$	100	3,1899	3,1887	2,7294
	200	5,2352	5,2273	4,898
	300	6,9462	6,9351	6,4877
	400	8,3512	8,3354	8,2123
	500	9,45795	9,4203	9,9373
	600	10,3131	10,2498	11,2345
	700	11,021	10,938	12,7535
	800	11,6591	11,5586	13,972
	900		12,1367	15,0412
	1000		12,6882	15,94
	1100		13,2154	17,0791
	1200		13,7207	17,75
Length $X_4 / S$	500	8,14	7,9725	8,028
	600	8,5053	8,345	8,5954
	700	8,9146	8,7304	9,9268
	800	9,5252	9,1504	11,082
	900		9,582	12,2283
	1000		9,997	13,43
	1100		10,4066	13,9844
	1200		10,8195	14,74
Length $X_5 / S$	500	13,165	13,2472	12,82
	600	15,798	15,8715	15,2265
	700	18,245	18,3265	17,3993
	800	20,3914	20,462	19,31
	900		22,6128	20,5593
	1000		24,71	21,5
	1100		26,745	22,3676
	1200		28,754	23,2

Figure 16 and 17 show the u-velocity component profiles along the channel for  $Re = 100$  using semi-staggered mesh with refinement 66x33 central differencing and UNIFAES. The development of the profile towards a parabola is apparent in both schemes.

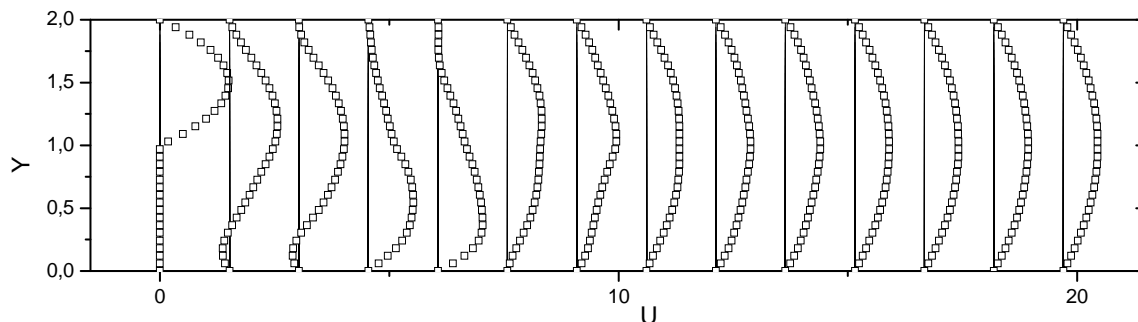


Figure 16 – Velocities profile using central scheme for Re = 100.

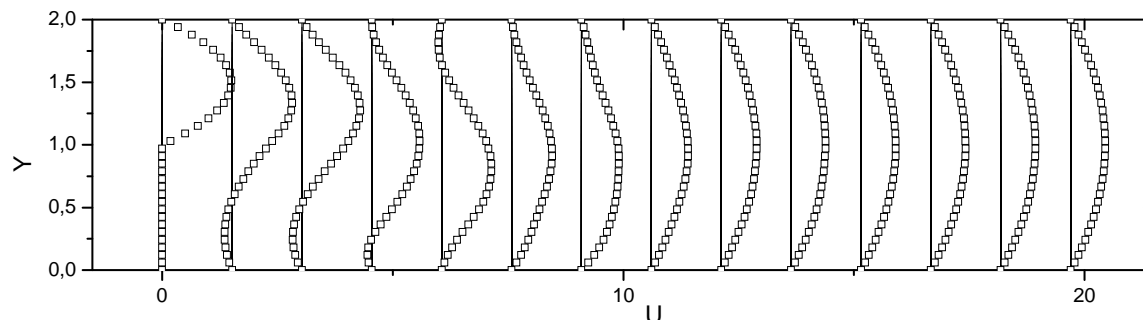


Figure 17 - Velocities profile using UNIFAES for Re = 100.

### 3. CONCLUSIONS

For the backward facing step problem, it was possible to solve the not diagonally dominant pressure equation of the semi-staggered mesh by means of the iterative method employing an appropriate under-relaxation factor. In other words, the lack of diagonal dominance of the pressure equations does not avoid the use of the semi-staggered mesh provided that adequate relaxation factors are applied.

The results with the central scheme, when converged, were very close to the results of UNIFAES.

With Reynolds from 600 on we can see a crescent difference between the numerical results of this work (with UNIFAES and central) and the experimental results of Armaly *et al.* (1983); this difference can be attributed to three-dimensional effects cited by Armaly *et al.* (1983).

### 4. ACKNOWLEDGEMENTS

The authors thank CNPq (National Council Scientific and Technological Develop) for the financial support in terms of a post-doctoral scholarship.

### 5. REFERENCES

- Armaly, B. F.; Durst, F.; Pereira, J. C. F. e Schönung, B., 1983, "Experimental and theoretical investigation of backward-facing step flow". *Journal of Fluid Mechanics*, v.127, p.473-496.
- Figueiredo, J. R. e Oliveira, K. P. M., 2009a, "Comparative study of UNIFAES and other finite-volume schemes for the discretization of advective and viscous fluxes in incompressible Navier-Stokes equations, using various mesh structures." *Numerical Heat Transfer Part B: Fundamentals*, v.55, n.5, p.379 - 405.
- Figueiredo, J. R. e Oliveira, K. P. M., 2009b, "Comparative study of the accuracy of the fundamental mesh structures for the numerical solution of incompressible Navier-Stokes equations in the two-dimensional cavity problem." *Numerical Heat Transfer, Part B: Fundamentals*, v.55, n.5, p.406-434.
- Kuznetsov B.G., 1968, "Numerical methods for solving some problems of fluid flow." *Fluid Dynamics Transactions*, 4:85-89.
- Oliveira, K. P. M., 2009, "Estudo comparativo de malhas e esquemas de discretização para as equações de Navier-Stokes em escoamentos incompressíveis." Ph.D. thesis, University State of Campinas.
- Rhie, C. M., e Chow, W. L., 1983, "Numerical study of the turbulent flow past an airfoil with trailing edge separation." *AIAA Journal*, v.21, n.11, p.1525-1532, 1983.

### 6. RESPONSIBILITY NOTICE

The authors are the only responsible for the printed material included in this paper.